



Energy and Nuclear Engineering Master Thesis

Selection of hydrothermal methods applied to SOFCs anodes recovery for hydrogen technologies at the end of life

Candidate

Fabio Iervolino

Supervisors

Smeacetto Federico

Fiorilli Sonia Lucia

Santarelli Massimo

Politecnico di Torino

December 2021

Abstract

In the actual context of growth of energy demand and sensibility to topics of sustainable development, in the environmental, economic and social spheres, the development and research of Solid Oxide Fuel Cell technologies, and hydrogen technologies in general, presents a concrete possibility to improve the capability to satisfy the needs of a market whose global relevance is stronger than ever, while meeting the requirements imposed from the legislators.

The goal of this work is to propose a selection of strategies and evaluate their effectiveness for recovering and recycling the materials from end-of-life Solid Oxide Fuel Cells. In particular, the possibility to obtain raw materials, in form of powders from the disassembling and treatment of the cells, that are suitable to be utilized for the production of new cells through hydrothermal treatments will be investigated.

Index

Abstract.....	3
List of tables.....	7
List of figures.....	7
List of acronyms.....	10
Introduction.....	13
BEST4Hy.....	13
Thesis.....	15
Fundamentals.....	19
Thermodynamic model of a fuel cell.....	19
Solid Oxide Fuel Cells.....	22
Anode.....	23
Cathode.....	24
Electrolyte.....	24
Interconnector plates.....	27
Supplier cell characterization.....	29
Methods: State of art and literature.....	30
Hydrothermal treatments.....	30
Nickel leaching.....	30
Acid Leaching.....	31
Chelation with EDTA.....	32

Methods: Experimental procedure.....	33
Cell disassembly.....	34
Sealant removal.....	34
Cathode recovery.....	34
Protective layer polishing.....	36
Electrolyte and anode milling.....	37
Hydrothermal treatment.....	38
Acid leaching with HNO ₃	40
EDTA Chelation.....	42
Acceptance Criteria.....	45
Results.....	46
Polishing.....	46
Milling.....	47
Hydrothermal treatment.....	48
Acid Leaching.....	51
Chelation.....	53
Mass balance.....	55
Conclusions.....	57
References.....	61

List of tables

Tab.1 – Acid leaching literature results: fractional weight changes after the treatment. [14]

Tab.2 – Acid leaching literature results: porosity changes after the treatment. [14]

Tab.3 – Acceptance criteria provided by industrial partner for the recovered materials (processed into powders) for recycling.

Tab.4 – ICP analysis results on hydrothermal supernatant.

Tab.5 – ICP analysis results on acid leaching supernatant.

Tab.6 - ICP analysis results on chelation treatment supernatant.

Tab.7 – Average mass losses for each procedure adopted.

List of figures

Fig.1 – BEST4Hy project schematic overview. [1]

Fig.2 – Thermodynamic model of fuel cells.

Fig. 3 – Typical Polarization curve of a fuel cell. [2]

Fig. 4 – Schematic representation of a Solid Oxide Fuel Cell working with hydrogen as fuel.

Fig. 5 – SEM backscattered electron micrographs of an anode supported cell with layer characterization. [3]

Fig. 6 – Polymorphism of Zirconia. [4]

Fig. 7 – Ionic conductivity of YSZ in function of the concentration of Y₂O₃, with variable temperature. [7]

Fig. 8 – Y₂O₃ ZrO₂ phase diagram. [7]

Fig.9 – Coefficient of thermal expansion in function of temperature and Y2O3 mol%. [8]

Fig.10 – Single repeating unit (SRU) of a SOFC stack representation.

Fig. 11 – Layer and material characterization of the End-of-life cells provided by the supplier.

Fig.12 – Acid leaching literature results: graphical representation of the Nickel peaks removal after the treatment. [14]

Fig.13 – Ni-EDTA complex formation. [15]

Fig.14 – Flowchart of the experimental procedure.

Fig.15 – End-of-life cell as received from supplier (a) and sealant removal (b).

Fig.16 – End-of-life cell in Distilled water bath for cathode scratching.

Fig.17 – Cathode powders recover after scratching and drying.

Fig.18 – Operation of polishing machine to erode protective layer (a) and effect detail on fragments: before (b) and after polishing (c).

Fig.19 – Milling jars: (a) after milling, (d) before milling; loaded milling machine (b) and sieving equipment (c).

Fig.20 – Assembled (a) and disassembled (b) lab scale hydrothermal reactor.

Fig.21 – Powders retrieval after hydrothermal treatment (a) and centrifugation equipment (b).

Fig.22 – Acid leaching equipment setup (a) and preliminary study of the effect of particle size on kinetics of the reaction (b).

Fig.23 – Powders before (a) and after (b) performing the acid leaching treatment.

Fig.24 – EDTA chelation treatment ongoing on two samples.

Fig.25 – Block diagram for the procedure of extraction of Nickel.

Fig.26 – EDS analysis results before polishing treatment.

Fig.27 – EDS analysis results comparison: before and after polishing.

Fig.28 – Effect of milling time evaluated through SEM and BET analysis.

Fig.29 – XRD analysis: Effect of milling on crystalline phase transformation and comparison with benchmark supplier powders.

Fig.30 – Effect of hydrothermal treatment on specific surface area in function of treatment time.

Fig.31 - XRD analysis: Effect of hydrothermal treatment on crystalline phase transformation.

Fig.32 – XRD analysis: effect of acid leaching treatment on powder samples processed with variable hydrothermal treatment times.

Fig.33 – EDS semi-quantitative elemental analysis: effect of HNO₃ on Nickel leaching.

Fig.34 – XRD analysis: effect of chelation treatment on powder samples processed with variable hydrothermal treatment times.

Fig.35 – EDS semi-quantitative elemental analysis: effect of EDTA chelation on Nickel leaching.

List of acronyms

BET Brunauer–Emmett–Teller

DLS Dynamic Light Scattering

EDS Energy-dispersive X-ray spectroscopy

EDTA Ethylenediaminetetraacetic acid calcium disodium salt hydrate

GDC Gadolinium-Doped Ceria

ICP Inductively Coupled Plasma

LCA Life Cycle Assessment

LCC Life-Cycle Cost

LSC Lanthanum-doped Strontium Cobalt Oxides

LSM Lanthanum-doped Strontium Manganese Oxides

OCV Open Circuit Voltage

PEMFC Proton Exchange Membrane Fuel Cell

PGM Platinum Group Materials

SEM Scanning Electron Microscope

SOFC Solid Oxide Fuel Cell

SSA Specific Surface Area

SRU Single Repeating Unit

XRD X-Ray Diffraction

YSZ Yttria-Stabilized Zirconia

Introduction

BEST4Hy

This thesis is based on part of the work accomplished at Politecnico di Torino from March to July 2021 on the BEST4Hy project, with the aim to develop sustainable solutions for recycling of end-of-life hydrogen technologies.

BEST4Hy is based on an international partnership between research institutes and industrial partners and has received European Union funding from the Fuel Cells and Hydrogen 2 Joint Undertaking under grant agreement No 101007216.

The objective of the BEST4Hy project is to develop and validate existing and novel recycling processes for PEMFC and SOFC technologies, which at the moment translates to reaching TRL5, that would ensure the maximization of recycling of critical raw materials including Platinum Group Materials (PGMs), rare earth elements, cobalt and nickel. In Fig.1 a schematic overview of the goals proposed in the BEST4Hy project is presented.

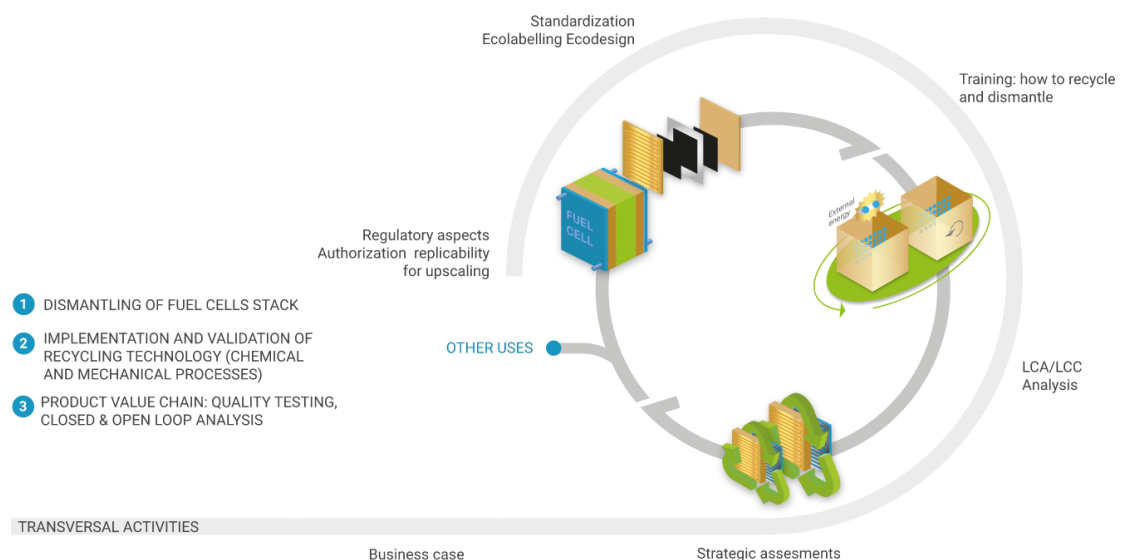


Fig.1 – BEST4Hy project schematic overview. [1]

The End-of-Life strategy is accompanied by LCC and LCA evaluations to ensure it delivers the best (in terms of cost effectiveness and environmental impact) materials for closed loop and

open loop recycling. At the end of the processes, the materials will be validated in terms of quality and performance when re-used in new components and in new stacks, demonstrating the overall efficiency of recycling in order to deliver a concrete validation of the circularity potential within the hydrogen device industry.

Further information and updates on this project can be retrieved on the official website. [1]

Thesis

The core goal of the thesis is the investigation of the possibility to treat with hydrothermal methods anodic materials of a SOFC reduced in form of powders, and to evaluate the effect on particle size and particle size distribution. The application of hydrothermal treatments to process Yttria-Stabilized Zirconia (YSZ), which is the main material component of the anode along with Nickel, is already consolidated but it is an innovation in the SOFC material recovery and recycling application.

The second goal is to provide an investigation of methods for the separation of Nickel from anodic materials, performing Nickel leaching both through acid and chelation with EDTA.

For this purpose, first of all, a brief description of the SOFC technology, in terms of physical model, conditions of operation, comparison with other similar technologies, components, materials, advantages and critical issues, will be provided to consent a better understanding of its fundamental features.

Additionally, after the characterization and the description of the particular cells provided by the supplier, a brief review of the state of art with reference to literature of the experimental procedures adopted, such as hydrothermal treatments, acid leaching and chelation with EDTA, will be presented.

Afterwards, beginning the experimental methods section, a description of the approach adopted to separate the components of the cell as provided by the supplier will be exposed, with the goal to describe how it is possible to access the anodic and electrolytic materials, which are the object of interest of the study.

Subsequently, the core investigation of the effect of hydrothermal treatments on particle size and particle size distribution will be reported. The following step will describe the results of the implementation of the two strategies presented for the separation of Nickel from YSZ.

Finally, after the assessment of the acceptance criteria, an overview of the results of each step of each procedure will be presented, to evaluate the successfulness of the approach, and eventual critical issues will be highlighted to consent future further optimization and a perspective on the design of a pilot-plant.

Fundamentals

Thermodynamic model of a fuel cell

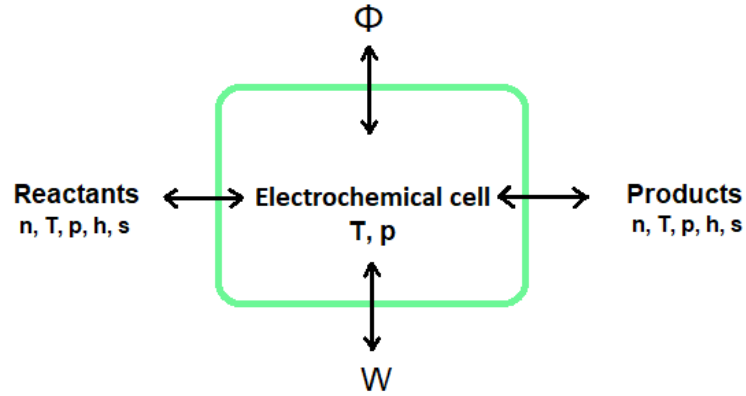


Fig.2 – Thermodynamic model of fuel cells.

By applying the first and second law of the thermodynamics as follows

$$\dot{\Phi} - W_{el} - \sum_P n_P h_P(T, p_i) + \sum_R n_R h_R(T, p_i) = 0$$

$$\frac{\dot{\Phi}}{T} - \sum_P n_P s_P(T, p_i) + \sum_R n_R s_R(T, p_i) = 0$$

and normalizing by the number of moles of the fuel fed to the cell, we can obtain that:

$$q - l - \sum_P \nu_P h_P(T, p_i) + \sum_R \nu_R h_R(T, p_i) = 0$$

$$\frac{q}{T} - \sum_P \nu_P s_P(T, p_i) + \sum_R \nu_R s_R(T, p_i) = 0$$

$$q - l - \Delta h_{reaction} = 0$$

$$\frac{q}{T} - \Delta s_{reaction} = 0$$

By combining the results obtained with the Faraday law, it is possible to deduce the Nernst equation which describes the voltage gradient across a cell in equilibrium conditions.

$$l = -[\Delta h_{react} - T\Delta s_{react}] = -\Delta g_{react}$$

$$l = \frac{W_{el}}{n_F} = \frac{I \cdot E}{z_F \cdot F}$$

$$E_{Nernst} = \frac{\pm \Delta g_{react}}{z_F \cdot F}$$

The behavior of the cell in non-equilibrium conditions is detailed in the following formula and graphical representation in Fig.3, with a brief description of the main losses which occur in a not-ideal device.

$$E = \frac{\pm \Delta g_{react}}{z_F \cdot F} + \frac{RT}{z_F \cdot F} \cdot \ln \frac{\prod_P (\frac{p_i}{p_0})^{v_i}}{\prod_R (\frac{p_i}{p_0})^{v_i}}$$

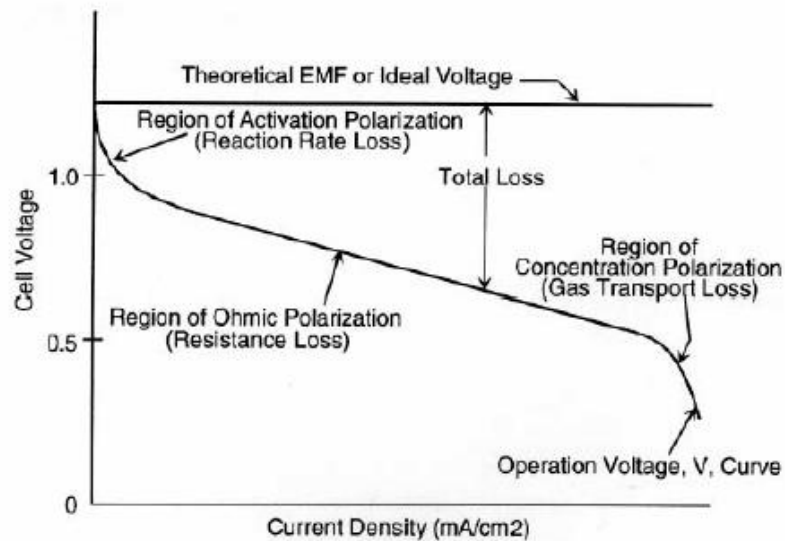


Fig.3 – Typical Polarization curve of a fuel cell. [2]

The modification of the ideal voltage is related to the charge transfer, charge migration (conduction and diffusion) and mass transport phenomena that occur in the device.

In SOFCs, thanks to the high temperatures involved, the activation and concentration losses are limited, therefore the behavior is prevalently resistive.

Solid Oxide Fuel Cells

Fuel cells are electrochemical conversion devices that produce electricity from the oxidization of a fuel. Solid Oxide Fuel Cells (SOFC) are a class of cells characterized by the electrolyte material, which is usually solid oxide or ceramic.

The working temperature is very high and can vary from 650 to 1000 °C. The high temperature has an important role in transport processes influencing positively the charge transfer, so the catalyst can be Nickel, which is cheap compared to Platinum, also featuring a higher tolerance to carbon fuels.

On the other hand, the high temperature results in the need for more expensive materials able to tolerate the working conditions and the degradation of the components is higher. Additionally, higher temperatures mean long startup and shutdown, increasing the transient operation time. For this reason, this technology is suitable for base load operations but not for fast transient applications such as transport.

This type of fuel cells also consents flexibility in the fuel choice and presents advantages like high efficiency, which can reach values of 60-70%, and long-term stability. Other positive aspects in common with all types of fuel cells are the null emissions in atmosphere, and the modular nature of the technology, which implies that performance does not scale with the size of the plant, and small plant applications are possible. In Fig.4 a hydrogen-fed SOFC is schematically represented.

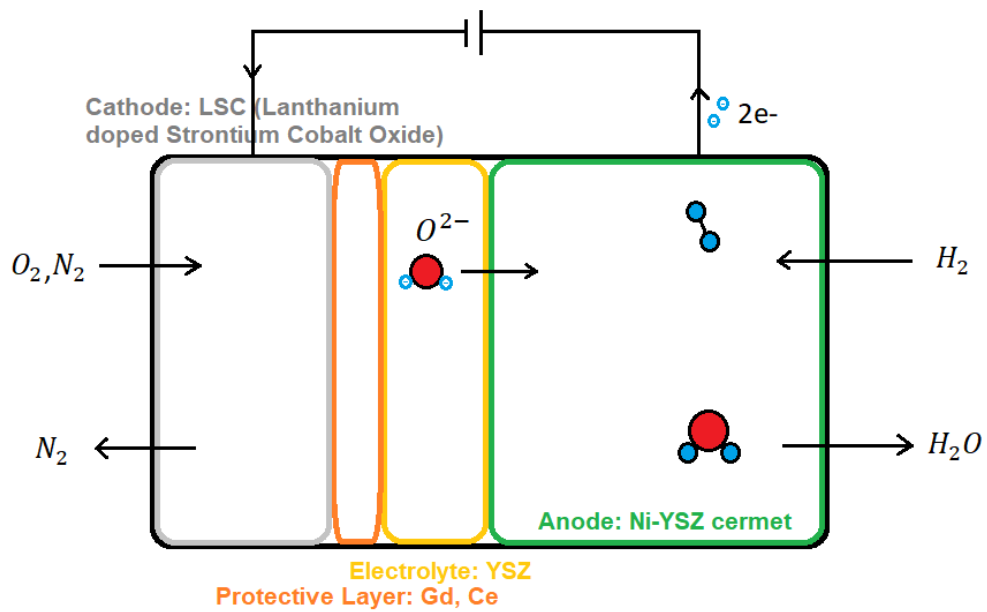
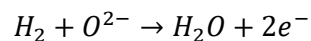


Fig.4 – Schematic representation of a Solid Oxide Fuel Cell working with hydrogen as fuel.

Anode

The anode is the place where O^{2-} ions that crossed the electrolyte combine with hydrogen H_2 (or a hydrocarbon fuel) to form H_2O and allow the separation of two electrons ($2e^-$), which are driven by a potential to the cathode, generating the electric current responsible for the electric output of the cell.



Because of its particular functions just explained, the anodic layer must provide a high catalytic activity, electronic and ionic conductivity with a sufficient porosity ($\sim 30\%$). The state of art material is Ni-YSZ cermet, with the anode covering the role of cell support (anode supported cells). In this configuration, the anode layer thickness is in the order of magnitude of 250-500 μm , whereas the electrolyte and the cathode layer thickness are respectively about 5 μm and 5-30 μm . In Fig.5 a SEM image of an anode supported SOFC is reported to consent a better idea of the proportions of the layers.

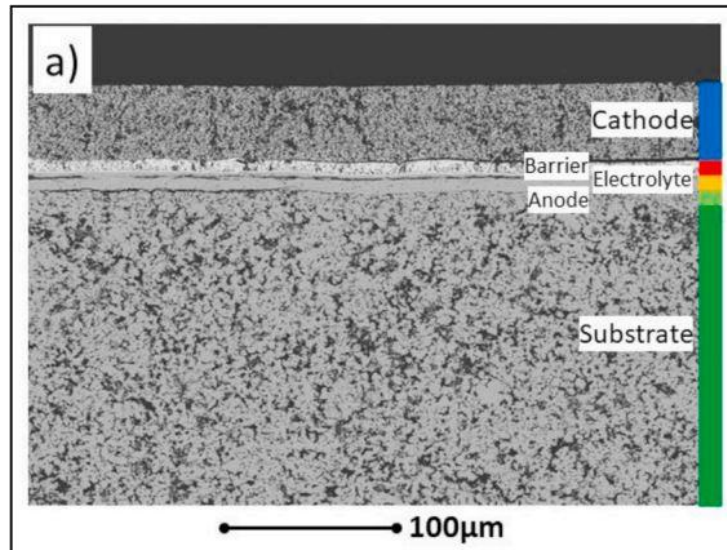
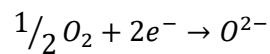


Fig.5 – SEM backscattered electron micrographs of an anode supported cell with layer characterization. [3]

Cathode

In the cathode the molecular oxygen O_2 combines with the electrons ($2e^-$) available from the anode, in order to form O^{2-} ions that will permeate through the electrolyte.



The material chosen for the cathode must feature similar characteristics with the anode, with the addition of a thermodynamical compatibility with YSZ composing the electrolyte. At the state of art, perovskites are often used as cathode layer materials, in particular Lanthanum-doped Strontium Manganese or Cobalt Oxides (LSM or LSC).

Electrolyte

The most common electrolyte material at the state of art is Ytria-stabilized Zirconia (YSZ), which is obtained doping ZrO_2 with Y_2O_3 . Obtaining stable sintered zirconia ceramic products is challenging mainly because of the volume expansion that accompanies the change of temperature and consequent shift from the various polymorphism configurations of its structure, reported in Fig.6, causing internal strains in the material. In fact, pure zirconium

dioxide undergoes a phase transformation from monoclinic crystal structure (stable at ambient temperature) to tetragonal and then to cubic approaching respectively 1170 °C and 2370 °C [4] [5].

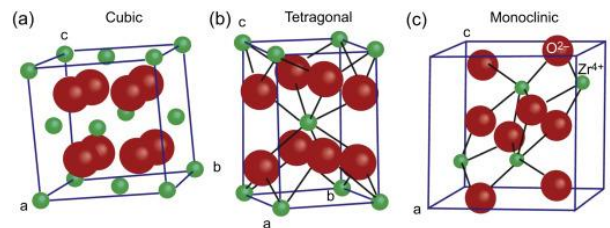


Fig.6 – Polymorphism of Zirconia. [4]

Therefore, YSZ is obtained processing pure zirconium dioxide with the substitution of some of the Zr^{4+} ions (ionic radius 0.82 Å) with slightly larger ions such as Y^{3+} (ionic radius 0.96 Å) [5]. The addition of two Y^{3+} ions generates a vacancy on the anionic sublattice, increasing the material ionic conductivity for O^{2-} ions. The system behavior exhibits a maximum of ionic conductivity followed by the decrease of ionic conductivity with further increasing Y doping as shown in the following plot in Fig.7.

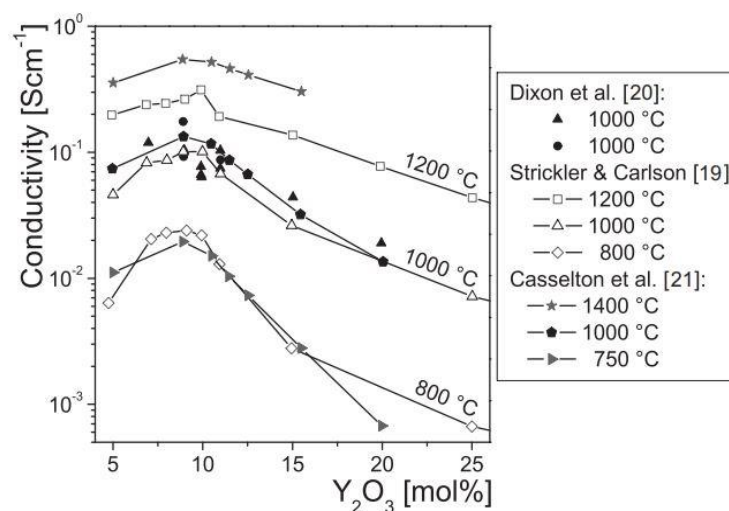


Fig.7 – Ionic conductivity of YSZ in function of the concentration of Y_2O_3 , with variable temperature. [7]

Although this plot highlights a peak performance, in terms of ionic conductivity, at a molar concentration of about 8% of Y_2O_3 for temperatures ranging from 800 to 1200 °C, in these conditions 8YSZ is situated in the 2-phase field (as visible in the diagram below), which can cause the material's decomposition into Y-enriched and depleted regions on the nm-scale and, consequently, the electrical performance degradation during operation. [7]

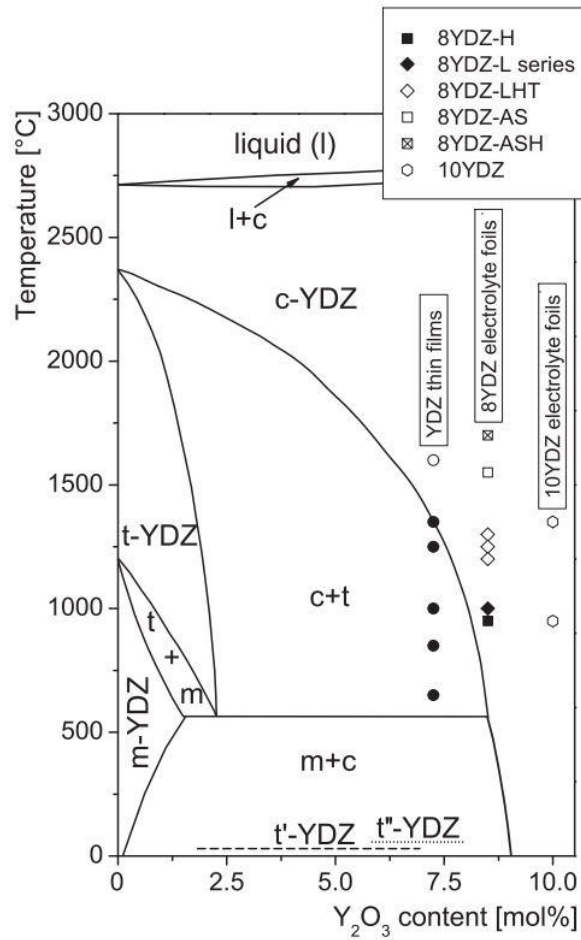


Fig. 8 – Y_2O_3 ZrO_2 phase diagram. [7]

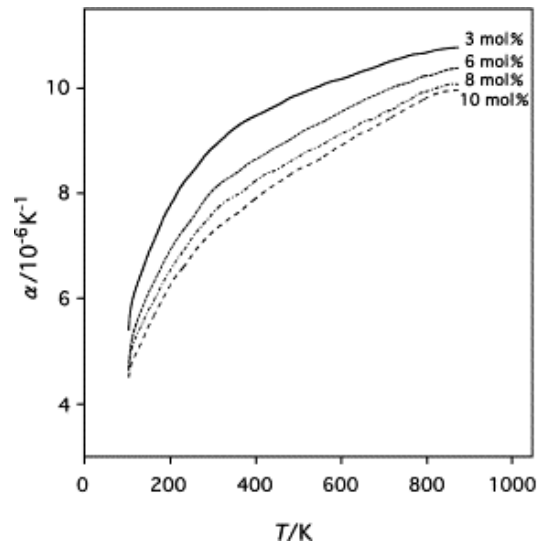
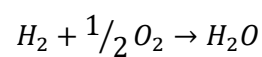


Fig.9 – Coefficient of thermal expansion in function of temperature and Y_2O_3 mol%. [8]

Another important aspect concerning the material choice of each layer is the compatibility between the thermal expansion coefficients, in order to avoid internal strains due to a mismatch of this parameter when the cell is subjected to the working conditions. In Fig.9 the coefficient of thermal expansion of YSZ in function of temperature and Y_2O_3 concentration is represented.

Interconnector plates

The current produced as electrical output in the cell depends on the quality of the cell in terms of current density, whereas the voltage is limited by the particular reaction that occurs inside the cell. In the case of hydrogen as a fuel, the reaction:



produces an Open Circuit Voltage (OCV) equal to 1.23 V, resulting in a cell output voltage that can vary in the range from 0.7 to 0.9 V. This value does not allow for an appropriate utilization in the sector of energy production. For this reason, fuel cells are allocated in a stack to obtain a suitable voltage through interconnector plates.

This component, represented in Fig.10, is critical because it must provide fuel and air input to the cells while maintaining the two streams insulated in order to avoid interactions that could result in explosions. Nonetheless, interconnector plates must be able to conduct electricity, their thermo-mechanical behavior should be sufficiently similar to the ceramic material in the cell while operating at high temperature (higher than 700°C), whilst being as cheap as possible. The state of art material is CROFER 22 APU, a stainless-steel alloy with 22% Cr, although, at high temperature, this material can experience Cr evaporation in contact with the cathodic atmosphere, forming CrO_2 which can deposit on the cathode surface deactivating it. This phenomenon is also known as Cr poisoning. [9] [10] [11]

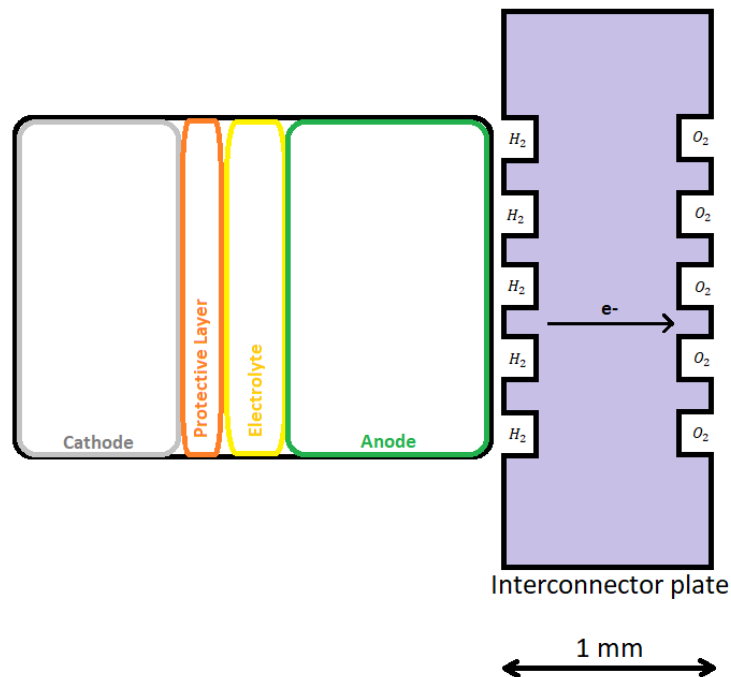


Fig.10 – Single repeating unit (SRU) of a SOFC stack representation.

Supplier cell characterization

A graphical representation of the end-of-life cells provided by the industrial partner is available in Fig.11, with a total thickness of 315 μm and a weight variable in the range 22.5-23.0 g. As it is possible to notice, the cathode layer is composed by LSC (Lanthanum-doped Strontium Cobalt Oxide), with a thickness of about 12 μm , then a protective layer made of GDC (Gadolinium-doped Ceria) is separating the cathode from the electrolyte. The latter is composed by YSZ (Yttria-stabilized Zirconia), with thickness that can vary from 3 to 6 μm , whereas the anodic material is a cermet of Nickel and YSZ.

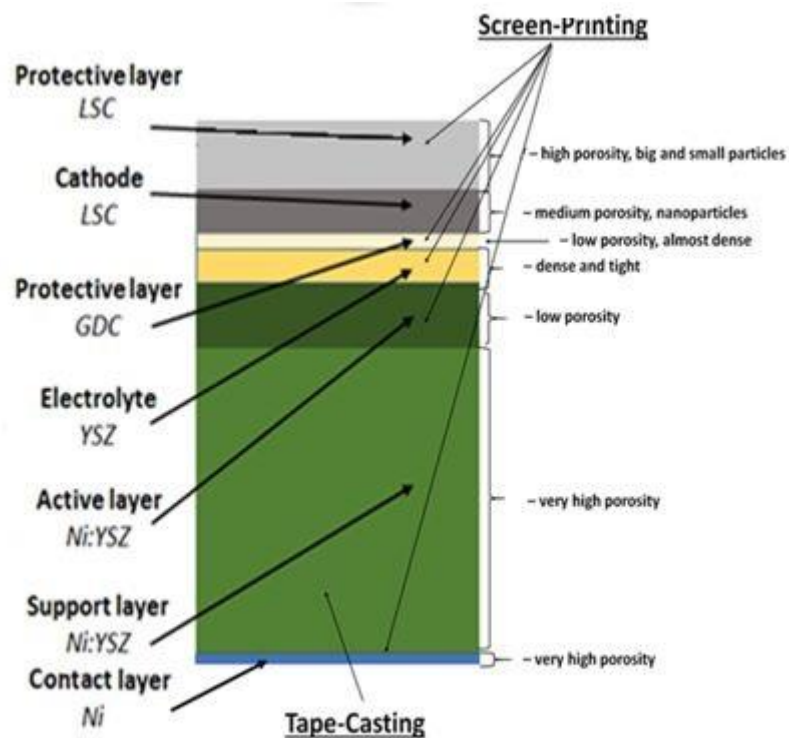


Fig. 11 – Layer and material characterization of the End-of-life cells provided by the supplier.

Methods: State of art and literature

In this section a brief description of the procedures adopted is presented, with reference to literature results that motivated the application of these techniques to the end-of-life SOFC material recovery.

Hydrothermal treatments

Hydrothermal methods consist in the use of an aqueous solution as a reaction system in a closed reaction vessel to create a high-temperature, high-pressure reaction environment by heating the reaction system. The goal is to induce a particle size reduction in the anodic material powders that are subjected to an environment at high pressure by heating the reaction vessel up to approximately 200°C, in order to limit the usage of mechanical energy which is already provided during the milling procedure.

The disintegration process of YSZ ceramics and phase transformation from tetragonal to monoclinic zirconia through hydrothermal treatments has already been successfully carried out and reported in literature [12] [13], but the application in the field of the recovery of anodic end-of-life SOFC materials is an innovation, because of the specific acceptance criteria in this field in terms of chemical purity, specific surface area and particle size distribution of the powders.

Nickel leaching

Another important objective is the investigation of the possibility to extract Nickel, the catalyst of the fuel cell, from the powders of YSZ and Ni-YSZ cermet. This result was obtained researching and conducting two different procedures retrieved by means of a literature review concerning the recovery of Nickel from exhausted batteries, electronic waste or spent catalyst. [14] [15]

Acid Leaching

The first procedure found in literature was more established and had already been used successfully for the extraction of Nickel without damaging the Zirconia in other applications. It consisted in exposing 0.5 g of Ni-YSZ wafers in 50 mL of 2.2M HNO_3 solution at 80°C for 2 h. The results of this approach (reported below) seemed appealing and reasonably easy to replicate. In the paper, a Nickel removal efficiency of about 90% and a porosity increase up to 20% were claimed, as it is possible to notice in Fig.12, Tab.1 and Tab.2. [14]

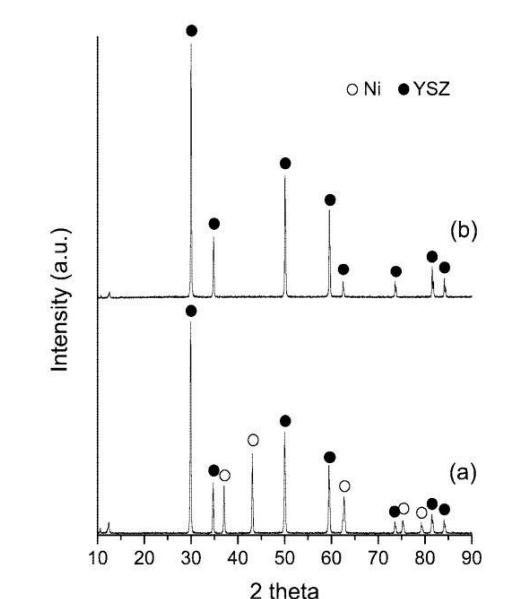


Table I. Fractional Weight Changes Observed for NiO/YSZ Composites after Reduction and after Leaching in HNO_3 [†]

YSZ/NiO mass ratio	Fractional weight after H_2 reduction	Fractional weight after leaching
100/0	0.999 (1.000)	0.999 (1.000)
80/20	0.959 (0.958)	0.805 (0.800)
60/40	0.916 (0.914)	0.605 (0.600)
50/50	0.894 (0.894)	0.501 (0.500)

[†]Values in parentheses were calculated based on complete reduction of NiO to nickel and complete removal of NiO.

Table II. Porosities of NiO/YSZ Samples after Various Pretreatment Conditions[†]

YSZ/NiO mass ratio	Initial porosity (%)	Porosity after H_2 reduction (%)	Porosity after leaching (%)
100/0	33	33 (33)	32 (33)
80/20	38	42 (41)	47 (47)
60/40	46	54 (54)	64 (64)
50/50	51	59 (60)	69 (72)

[†]Values in parentheses are calculated from initial porosities, assuming bulk densities for each component and complete reduction of NiO to nickel and complete removal of NiO.

Fig.12 – Acid leaching literature results: graphical representation of the Nickel peaks removal after the treatment. [14]

Tab.1 – Acid leaching literature results: fractional weight changes after the treatment. [14]

Tab.2 – Acid leaching literature results: porosity changes after the treatment. [14]

Chelation with EDTA

A second method, traditionally used for soil remediation and known as chelation, which is the formation of chelate complexes between a metal and the chelating ligand, was considered. Chelating agents are the most effective extractants that can be introduced in the soil washing process to enhance the extraction of heavy metals from contaminated soils. [15] [16] The advantages of chelating agents in soil cleanup include high efficiency of metal extraction, high thermodynamic stability, good solubility of the metal complexes formed and low adsorption of the chelating agents on soils. As a noncorrosive, nonhazardous application with the ability to remove metals from substrates effectively, this chelating property could be used advantageously for Ni recovery from the anodic and electrolyte material powders.

The choice of EDTA, an Amino poly carboxylic acid chelating agent, as a reagent to perform chelation, was due to the capacity to form a stronger bond with metallic ions than polyphosphates while operating effectively on a wider pH range than hydrolytic and acid types. [15]

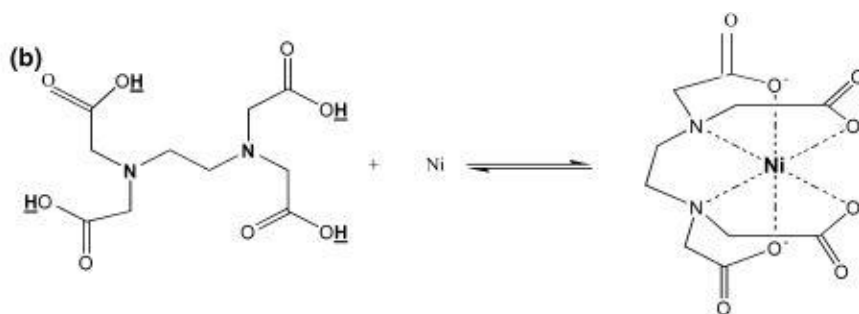


Fig.13 – Ni-EDTA complex formation. [15]

Methods: Experimental procedure

In this section, the whole experimental procedure followed is presented and discussed in terms of practical approach and issues, with the intention of describing all the procedures, the equipment and the conditions of operation adopted, highlighting eventual criticalities and observations found in laboratory application. In Fig.14 a flowchart representation is provided, where the whole processing of the end-of-life cells is summarized in 5 steps before accessing to recovered materials ready for the manufacturing of new cells.

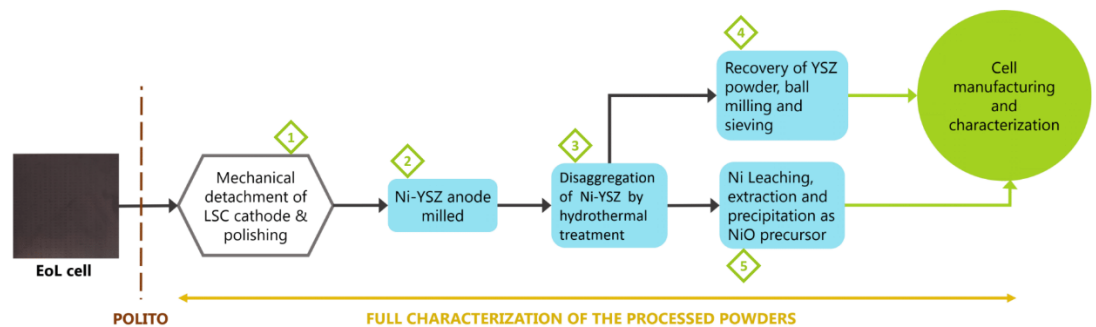


Fig.14 – Flowchart of the experimental procedure.

Cell disassembly

Before the anode material is accessible and available to be manipulated into powders, three preliminary steps have been followed in order to separate cathode and remove protective layer from electrolyte and anode. At each step a weight measurement was performed to assess the related material losses.

Sealant removal

The first step consisted in the manual separation of the edge sealing material of the cell, performed with a simple cutter, as shown in Fig.15.

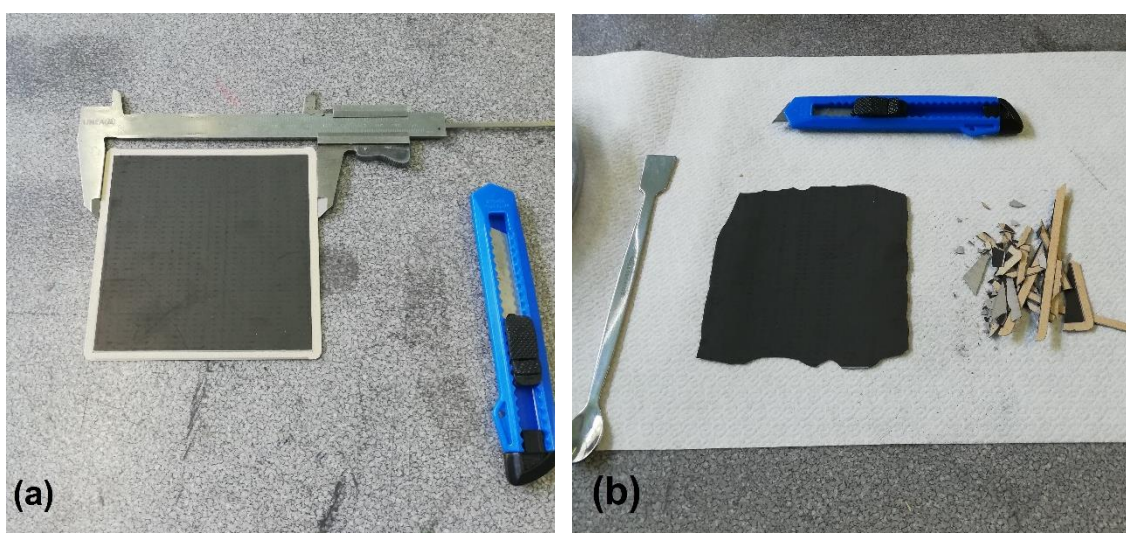


Fig.15 – End-of-life cell as received from supplier (a) and sealant removal (b).

Cathode recovery

As already highlighted, the cathode material provided from our supplier of end-of-life cells is LSC. The process of cathode layer separation has been carried out manually with a spatula in a distilled water bath, to avoid powder dispersion in ambient air and to facilitate its detachment. After allowing the scratched cathode powders to settle, they were retrieved by removing manually the majority of distilled water bath and successive drying in a heater at about 50°C. The cathode powders were then weighted, sampled and stored.

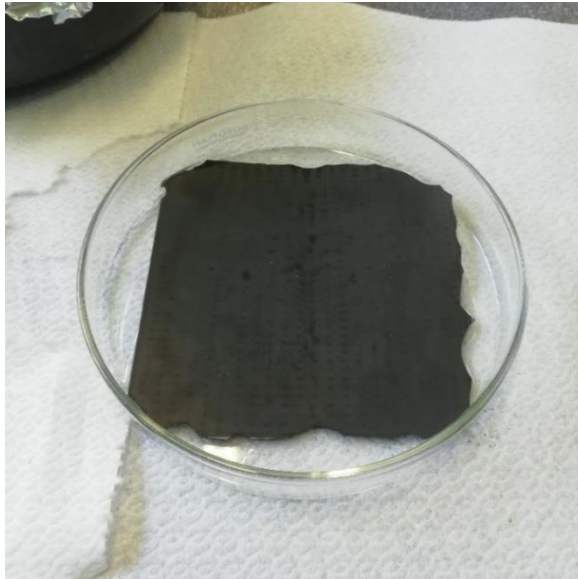


Fig.16 – End-of-life cell in Distilled water bath for cathode scratching.



Fig.17 – Cathode powders recover after scratching and drying.

The manual scratching has given successful results in terms of effectiveness of cathode layer removal, but it is obviously not suited in a perspective for a larger scale automated plant. Additionally, given the thinness of the cells and the fragility peculiar of ceramic materials, this step can lead to the cracking of the cell and consequent loss of material. Anyway, at laboratory scale and at this early stage of research, this approach represented the only possibility available.

Protective layer polishing

After the cathode detachment, the last preliminary step to access to electrolyte and anode material is the removal of the protective layer (Gadolinium-doped Ceria) deposited between the cathode and the electrolyte. This thin layer was not successfully removed with simple scratching. The first approach taken into account to separate this layer was manual polishing of fragments of half cells (cells whose cathode layer was removed) with sandpaper, but the results were poor. The optimized strategy featured the utilization of a water-assisted polishing machine by means of SiC grinding papers at increasing grit (320, 600 and 800), to avoid excessive removal of electrolyte along with the protective layer.

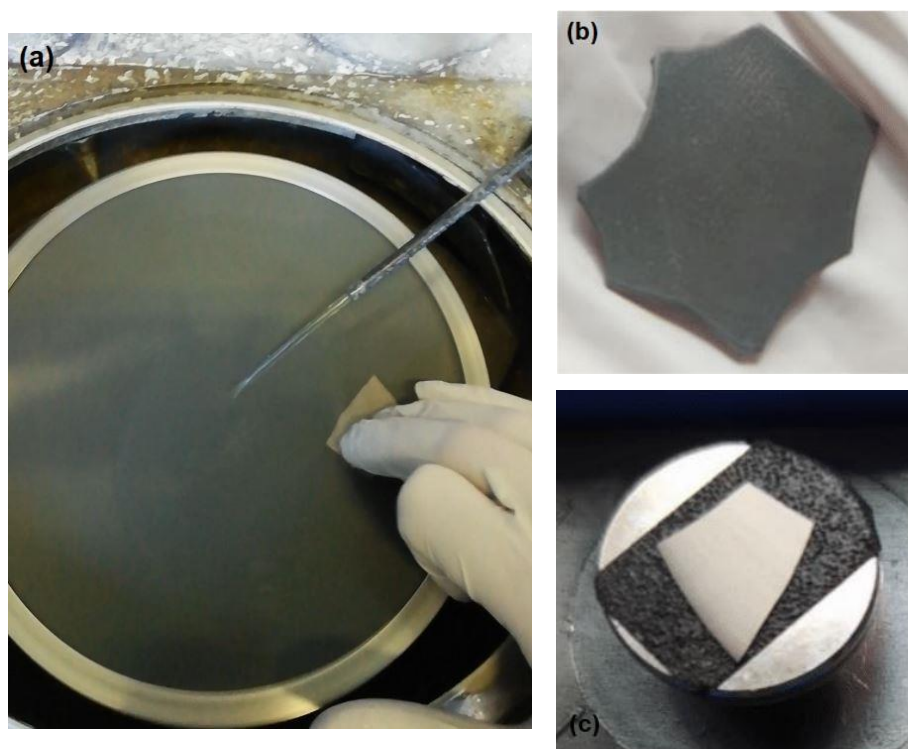


Fig.18 – Operation of polishing machine to erode protective layer (a) and effect detail on fragments: before (b) and after polishing (c).

The effectiveness of this procedure was evaluated through EDS analysis comparison of samples before and after polishing treatment, to assess the complete removal of GDC and cathode residuals.

Electrolyte and anode milling

Once all the preliminary steps were completed, the cells fragments were composed of their electrolyte (YSZ) and anode (Ni-YSZ) and were available to be reduced into powders through milling. This procedure was performed with the utilization of a sphere grinding machine (ball mill). A first selection of a single-sphere Tungsten Carbide grinder resulted in poor performance in terms of powder size distribution, and successive milling and sieving iterations were required in order to obtain a sufficient amount of powder with size below 25 μm . Therefore, a new alumina grinder with 6 spheres was selected and allowed a much more efficient milling procedure in terms of particle size reduction and distribution, as well as of quantity of powders with diameter inferior to 25 μm after sieving and successive weighting.

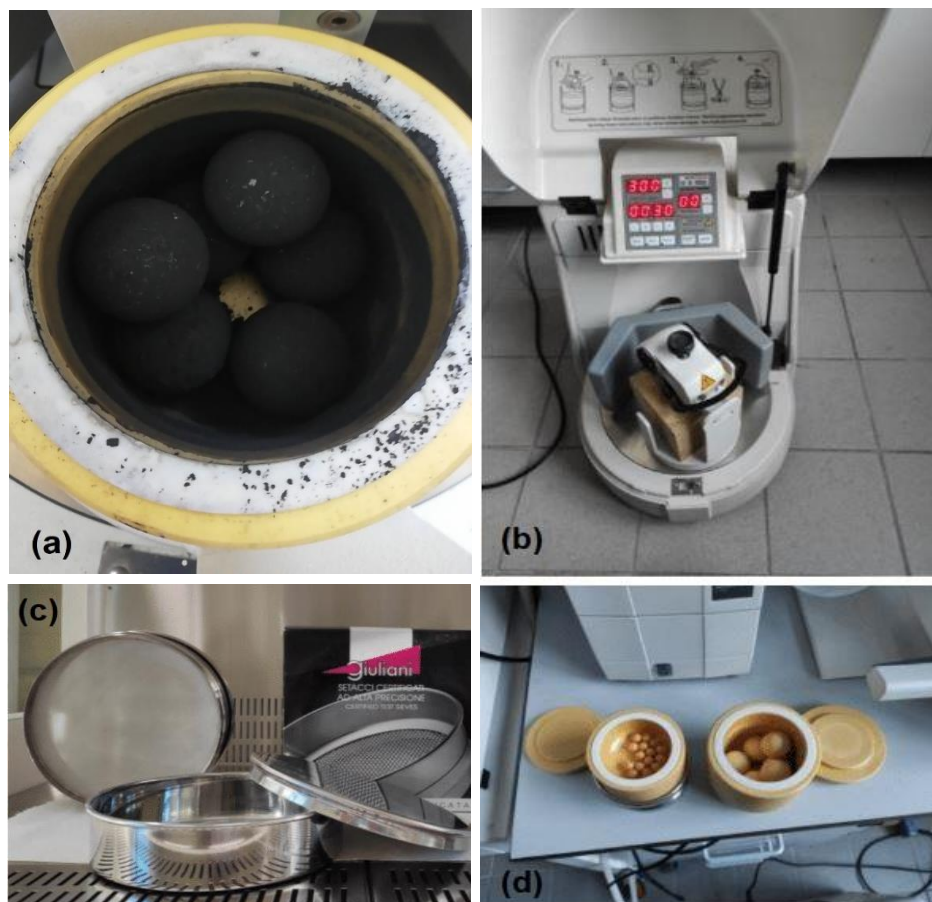


Fig.19 – Milling jars: (a) after milling, (d) before milling; loaded milling machine (b) and sieving equipment (c).

In Fig.18 the equipment for milling and sieving procedure is reported. The milling time was set to 6 hours at 450 rpm after the exploration of the effect of different milling times was preliminarily performed in the Tungsten Carbide grinder.

Additionally, the goal was to obtain a sufficient reduction in terms of particle size without relying on excessive milling times to avoid higher energy consumption.

After milling, powder characterization was performed by SEM/EDS, BET and XRD analysis.

Hydrothermal treatment

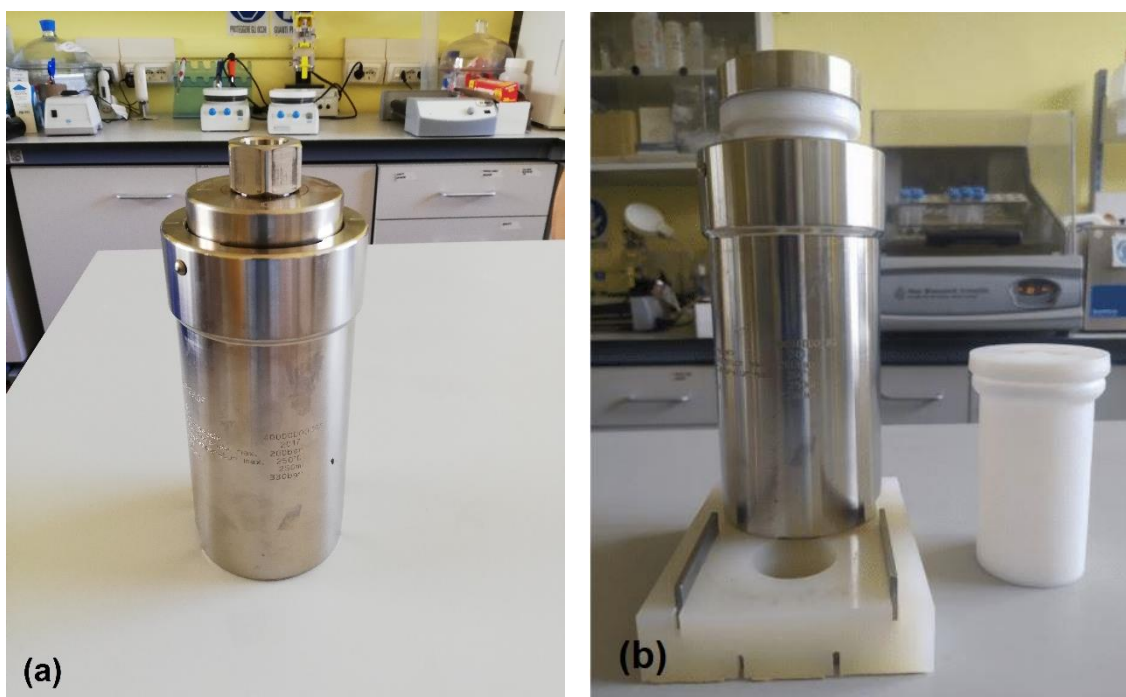


Fig.20 – Assembled (a) and disassembled (b) lab scale hydrothermal reactor.

As visible in Fig.19, the reactor main components are a Teflon recipient in which the water and the powders are located, and a steel vessel sealed with a screw. The hydrothermal conditions set included a temperature of 200°C, for a time variable from 2, 4, 6 and up to 12 hours, in order to assess the optimal value of treatment time. Under these conditions, each treatment was carried out with 2 g of anode-electrolyte powders in 105 mL of water, which corresponded to 50% of reactor volume.

After performing the hydrothermal treatment, the supernatant was recovered and characterized through ICP analysis, in order to quantify the amount of Nickel leaching and to investigate any possible residual cathodic or GDC material or contaminant.

Afterwards, the treated powders were recovered through multiple washing and centrifugation steps at 13000 rpm for 5 minutes and, finally, through drying in a heater at about 70°C. The centrifugation process has revealed to be very efficient, but also energy demanding. The study of alternative solutions to recover the powders in form of a slurry could be investigated and lead to significative savings in term of energy (therefore costs and emissions) and time. In Fig.20 pictures relative to the unloaded hydrothermal reactor before retrieving the powders and the centrifugation machine are reported.

The effectiveness of the treatment in terms of particle size reduction was investigated on the retrieved powders through BET, to evaluate specific surface area, and DLS analysis, to evaluate grain size distribution.

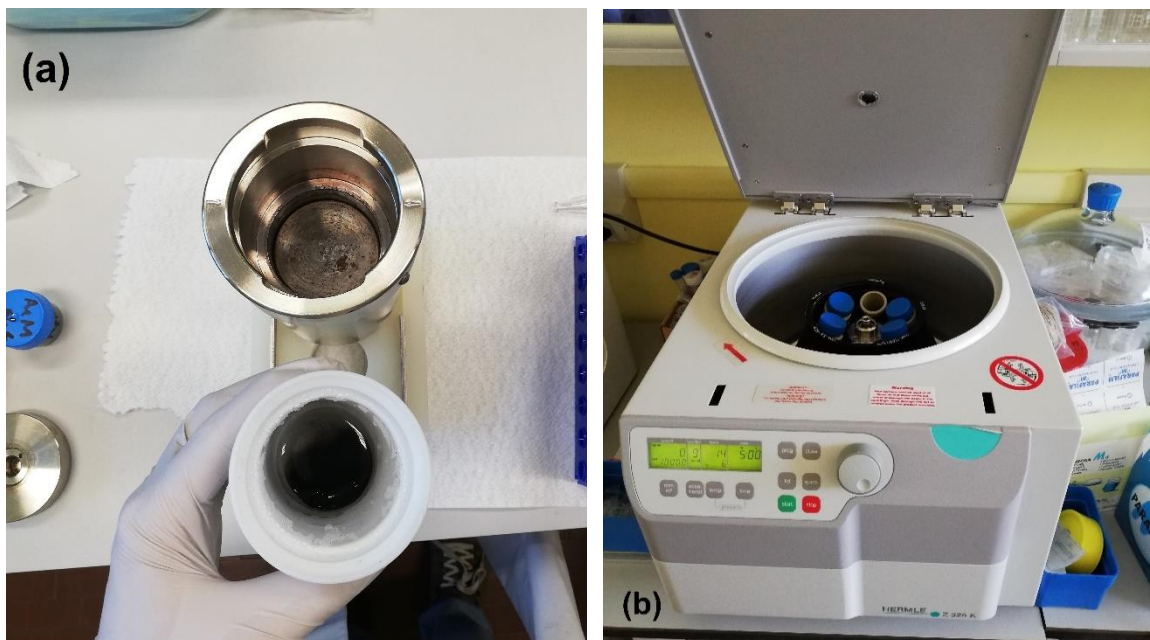


Fig.21 – Powders retrieval after hydrothermal treatment (a) and centrifugation equipment

(b).

Acid leaching with HNO_3

As the reference literature work was performed on Ni-YSZ wafers, it was reasonable to expect even better results when operating with powders of the same material, given the increase of area of contact between nitric acid solution and Ni-YSZ when using powders. The applied conditions were in the same solid-to-liquid proportions as literature: 1 g of powders of Ni-YSZ were treated in 100 mL of 2.2M HNO_3 solution at 80°C for 2 h, with the addition of stirring performed at about 600 rpm. The literature case was implemented on bulk wafers in acid bath, whereas the powder treatment was carried out in a glass recipient in which the nitric acid solution was, in this order, poured and heated on a heating and stirring plate until reaching the set temperature of 80°C. In order to obtain a homogeneous heating across the whole recipient, the latter was inserted in a bath of silicone oil (Dimetil silossano, trimetilsilossi-terminato), which helped with the control of temperature of the treatment supported with a thermometer. Once the set temperature had been reached, the Ni-YSZ powders were inserted in the recipient to start the treatment. During the 2 hours, periodical checks on the temperature assured a stable value around 80°C. The experimental setup adopted is available in Fig.21.

At the end of the acid exposure, the recipients were left to cool until they were safely manageable. At this point, the supernatant was extracted, collected in vials, filtered and diluted properly for ICP analysis, to investigate the effectiveness of the Nickel leaching. For what concerns the powders, the retrieving procedure followed successive steps of washing, to eliminate eventual residual nitric acid and derivatives, centrifugation and final drying. The mass losses in these steps were considerable, in the order of magnitude of 30%, but as already said at this early stage of research and at laboratory scale, to evaluate the effectiveness of the procedure, this approach was considered the best option available. In Fig.22 it is noticeable a qualitative change of the color of the powders after the treatment was concluded.

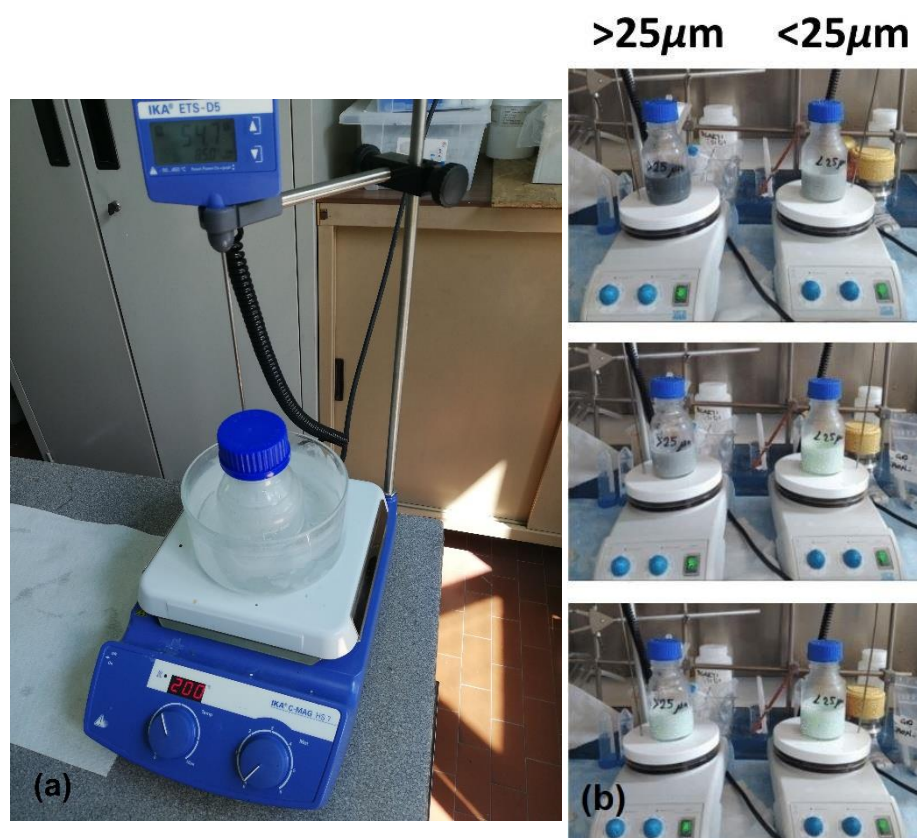


Fig.22 – Acid leaching equipment setup (a) and preliminary study of the effect of particle size on kinetics of the reaction (b): the advancement of the reaction is noticeable with the change of color of the powders from black to green. As it is clearly noticeable, the reaction is considerably faster for particles with size lower than 25 µm.

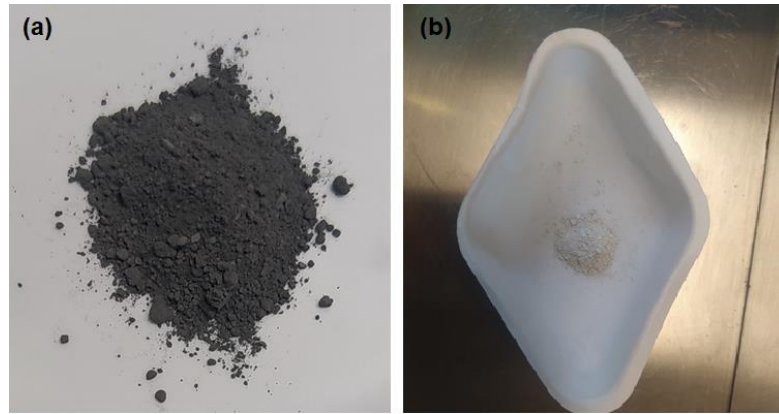


Fig.23 – Powders before (a) and after (b) performing the acid leaching treatment.

Powder characterization after the treatment was carried out through XRD/XRF, ICP, SEM/EDS and weight analysis.

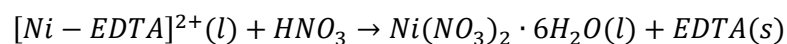
EDTA Chelation

Chelation under atmospheric reflux conditions was performed at the optimized conditions reported on the relative article, more in detail: EDTA solution 0.8M concentrated, temperature equal to 80°C and stirring speed of about 600 rpm by means of heating and stirring plate and silicone oil, solid to liquid ratio equal to 1/25 on a powder sample of 1 g. The EDTA solution was prepared adding NaOH until complete dissolution and pH = 11.0, in order to deprotonate carboxylic groups and allow chelation. The temperature limitation was set by the boiling point of the suspension, because of the atmospheric pressure. In Fig.23 the procedure equipment while ongoing treatment is reported.

After chelation, the possibility of separating the Metal-chelate complex (liquid phase), which was blue in color, and the residual YSZ (precipitate) through filters was explored.

Although this was the strategy adopted on literature, the utilization of a sintering funnel resulted in the irremediable loss of the majority of the powders, which were trapped inside the filter. The identical result was obtained when filtering was conducted with a syringe filter with pores of 20 μm . Therefore, in order to avoid considerable losses of the smaller fraction

of powders, the method featuring three successive centrifugations and distilled water rinses was selected.



The metal-chelate complex was set to dechelation by nitric acid (EDTA was separated, and nickel was extracted as nickel nitrate) and ICP characterization, whereas the precipitate residue was dried and characterized through XRD/XRF, SEM/EDS and weight analysis.



Fig.24 – EDTA chelation treatment ongoing on two samples.

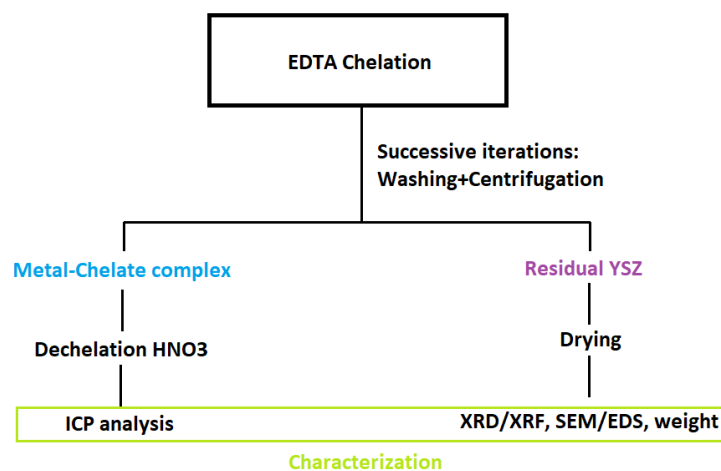


Fig.25 – Block diagram for the procedure of extraction of Nickel.

Acceptance Criteria

For what concerns acceptance criteria to assess the successfulness of the implementation of the experimental procedure to the half-cell materials, those were delivered by BEST4Hy industrial partners. In particular, acceptance criteria are related to chemical purity, specific surface area and particle size distribution of the powders, as reported more in detail below in Tab.3.

Compound	Chemical Purity, %	Specific Surface Area, m ² /g	Particle Size Distribution, μm	Comments
NiO	>99	3-3.5	0.4-1 D ₅₀ ~0.7	Wider PSD is possible, but to avoid a lot of too big and too small particles.
YSZ	>99	12-20	0.1-0.6 D ₅₀ ~0.3	In cell we use both, 3YSZ and 8YSZ (negligible amount). Focus on 3YSZ

Tab.3 – Acceptance criteria provided by industrial partner for the recovered materials (processed into powders) for recycling.

As revealed from the supplier, the presence of impurities is dangerous because it can affect the performance of the cell. For what concerns the specific surface area, it is related to the sinterability of the cells and this parameter heavily depends on particle size distribution. Additionally, particle size distribution is an important parameter because of its direct influence on sintering properties and thus on the electrochemical performance of the cell.

Results

Polishing

As it is clearly visible from the results in Fig.25 and Fig.26, the polishing procedure adopted resulted in an irrelevant concentration of the components of the GDC protective layer between cathode and electrolyte, and no further relevant presence of cathodic material was revealed. It is possible to conclude that the polishing procedure is reliable and efficient, although time demanding. It is also important to consider that, given the particular procedure adopted, some of the electrolyte material might have been removed along with the other layers.

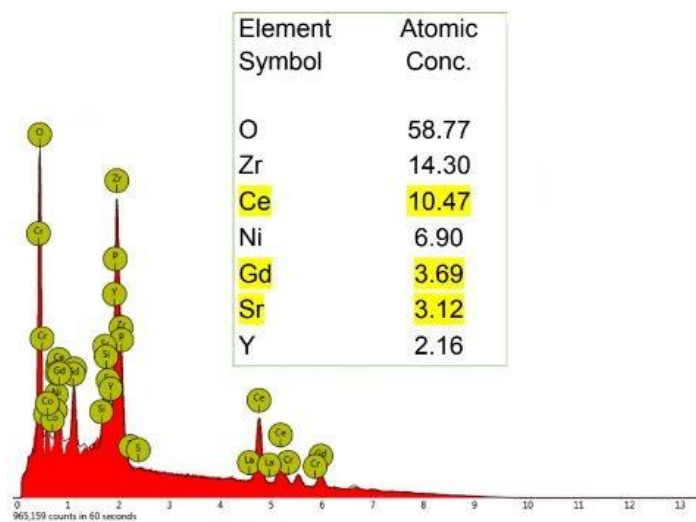


Fig.26 – EDS analysis results before polishing treatment.

EDS semi-quantitative elemental analysis

Before polishing

After polishing

	Atomic conc.	Atomic conc.
Ni	6.90	52.68
Zr	14.30	17.36
O	58.77	27.06
Y	2.16	1.51
Ce	10.47	ND
Gd	3.69	ND
Sr	3.12	ND

Fig.27 – EDS analysis results comparison: before and after polishing.

Milling

The milling procedure optimization, given a set milling equipment, depends on milling time and rotational speed of the device and on the number of milling spheres. Considered that increasing the latter increases the mechanical energy to which the material is subjected, it is safe to affirm that increasing the value of this parameter would result in a faster reduction of powder size or in a higher quantity of smaller powders within the same time of operation. The effect of milling time at 450 rpm on particle size reduction was studied evaluating the specific surface area through BET analysis and through SEM evaluation of the particle size range. The results are presented in Fig.26.

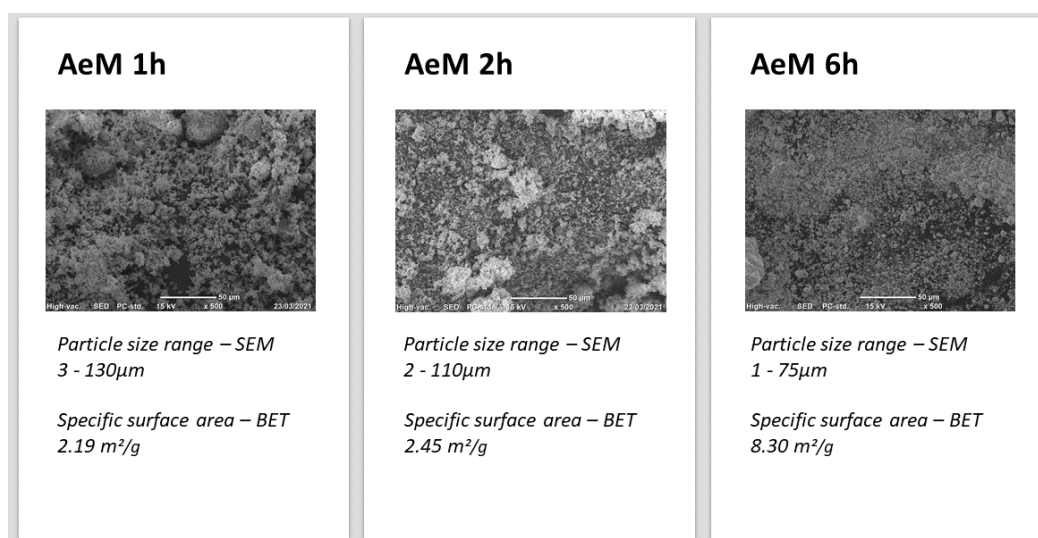


Fig.28 – Effect of milling time evaluated through SEM and BET analysis.

As expected, the increase in milling time resulted in an increase of the specific surface area and an overall decrease in particle size. Considered the result obtained, the set milling time for further treatment was 6 hours at 450 rpm.

An interesting point that was revealed from X-ray diffraction analysis is the crystalline phase transformation from cubic to monoclinic induced by the mechanical energy provided during

milling. As it is possible to notice from Fig.27, the cubic crystalline phase peaks decrease their amplitude, whereas monoclinic phase peaks increase in magnitude.

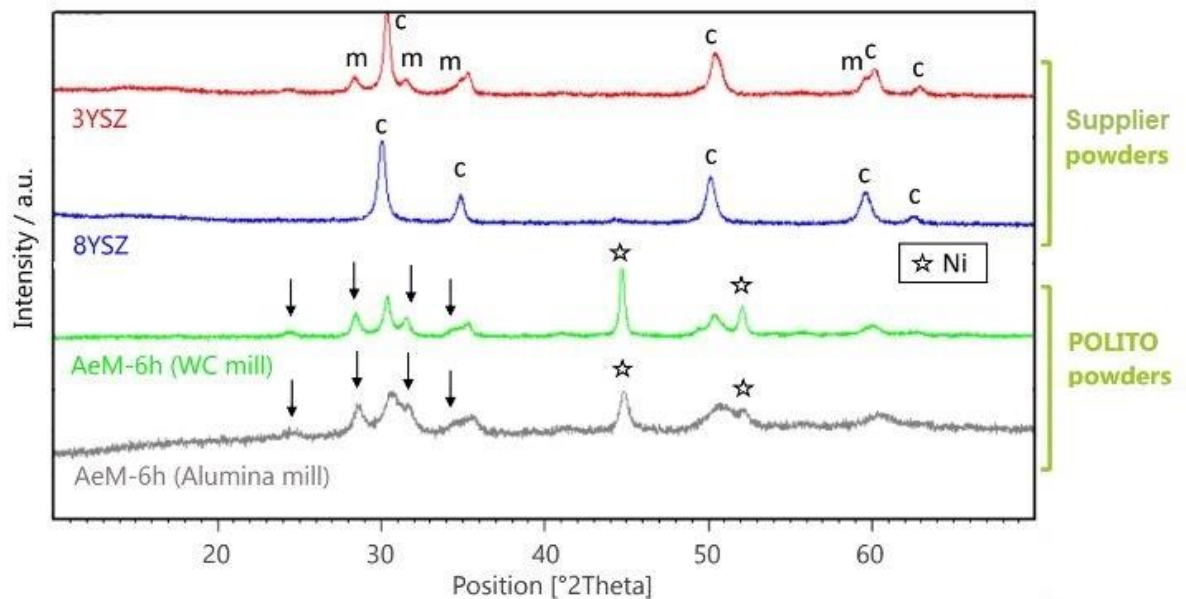


Fig.29 – XRD analysis: Effect of milling on crystalline phase transformation and comparison with benchmark supplier powders.

In conclusion, a crystalline phase transformation is induced from cubic to monoclinic. The values of particle size range and specific surface area obtained through simple milling for 6h at 450 rpm do not meet the requirements, accordingly with the expectations, since one of the experimental procedure goals is to evaluate the possibility to meet the criteria of success through hydrothermal treatments.

Hydrothermal treatment

The hydrothermal treatment was performed on powders that underwent milling for 6 hours at 450 rpm in the alumina ball mill with 6 milling spheres, and successive sieving to separate the grains with size inferior to 25 μm . The target was the investigation of the possibility to induce further particle size reduction of 2 g of powders in a closed reactor by setting the

temperature at 200°C with consequent increase of water/steam pressure. The effectiveness of the treatment at variable times was evaluated by means of BET and DLS analysis.

As it is noticeable from the results in Fig.28, the hydrothermal treatment successfully reduced the particle size of the powders, given the increase in specific surface area. An interesting observation that can be extrapolated is that the increase in SSA is relevant until 4 hours of treatment, then a further increase of treatment time does not provide enough increase of SSA to justify the choice. From the energy balance point of view this is important because the increase of time of treatment at 200°C determines a consequent increase in energy and time consumption of the process. Thanks to X-ray diffraction analysis in Fig.29, it is possible to affirm that the treatment did not induce any further crystalline phase transformation, since the position and the amplitude of the cubic crystalline phase and monoclinic phase peaks did not change.

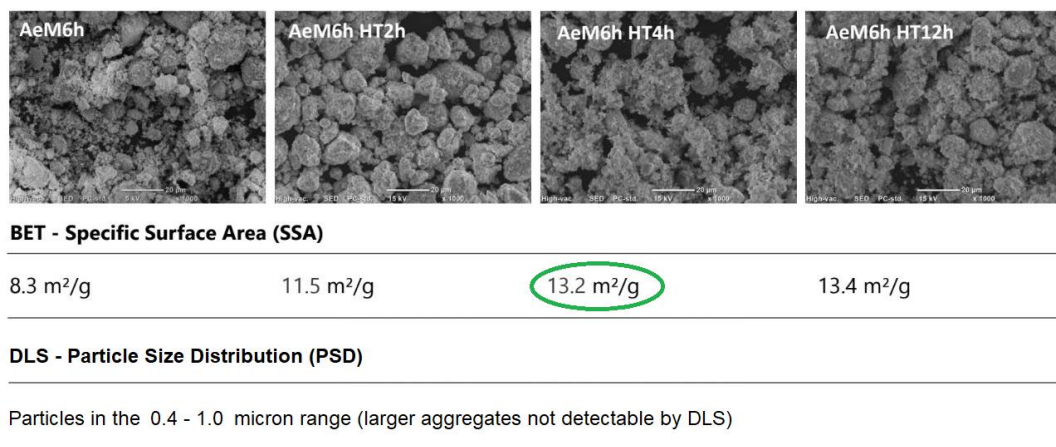


Fig.30 – Effect of hydrothermal treatment on specific surface area in function of treatment time.

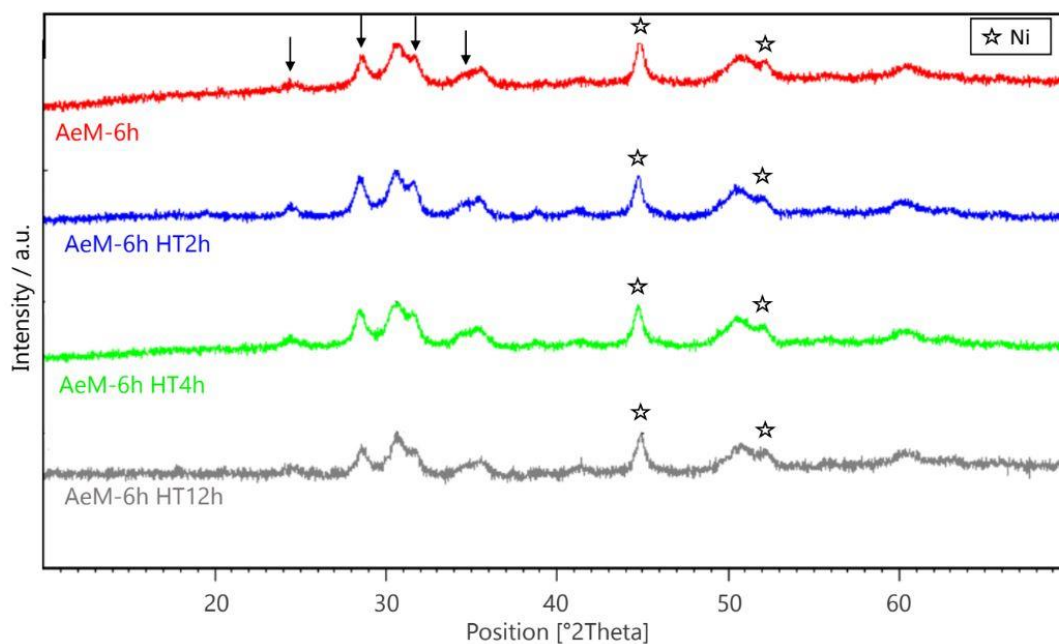


Fig.31 - XRD analysis: Effect of hydrothermal treatment on crystalline phase transformation.

For what concerns the supernatant collected after the treatment, ICP analysis was performed to investigate the eventuality of nickel leach inside the reactor. The results are reported in Tab.4. As it is clearly noticeable, a negligible amount (order of magnitude of 1 ppm) of Nickel is subjected to leaching in the hydrothermal treatment; YSZ instead is not affected.

ICP quantitative elemental analysis [ppm]	Ni	Y	Zr
HT2h	0.4	0	0
HT4h	1.1	0	0
HT12h	1.7	0	0

Tab.4 – ICP analysis results on hydrothermal supernatant.

It is safe to affirm that performing the hydrothermal treatment under the optimized conditions (4h, 200°C), the requirements in terms of specific surface area and particle size

distribution are met, while no further crystalline phase transformation and no Nickel leaching phenomena are induced.

Acid Leaching

Acid leaching was performed on samples of 1 g of powders of Ni-YSZ, treated in 100 mL of 2.2M HNO_3 solution at 80°C for 2 h at about 600 rpm stirring. As it is reported in Fig.31, the XRD analysis on variable time of hydrothermal treatment samples evidences the complete extraction of Nickel from the powders in all samples. In fact, the peaks corresponding to Nickel are removed in each curve. No significant variation in extraction effectiveness is relatable to higher hydrothermal treatment time since the Nickel peaks disappear completely even with no hydrothermal processing.

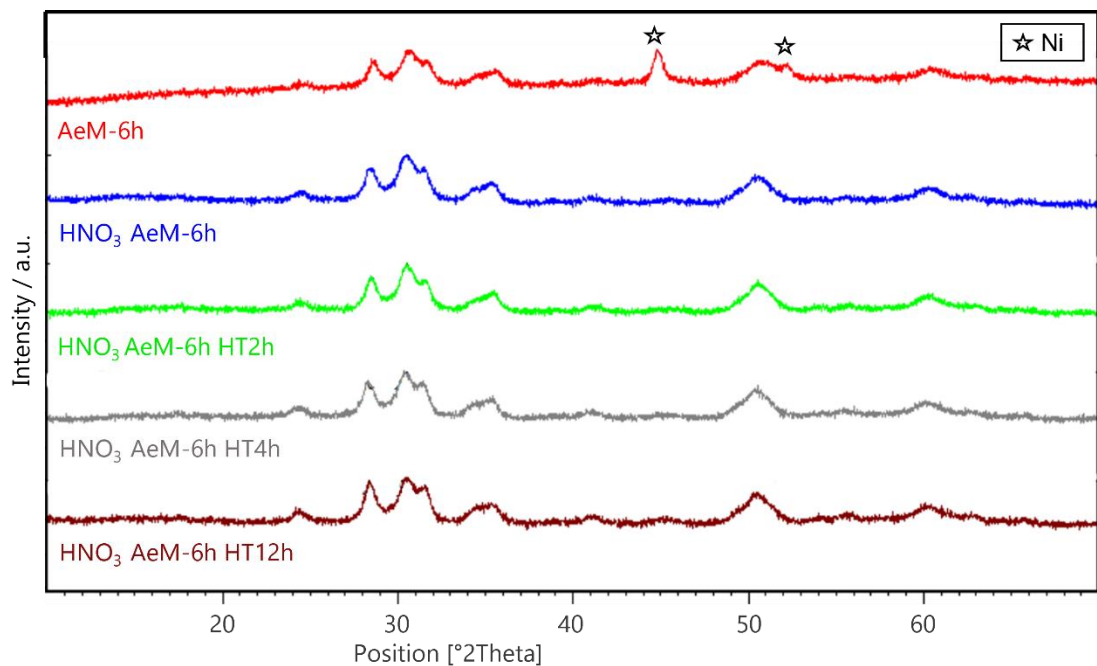


Fig.32 – XRD analysis: effect of acid leaching treatment on powder samples processed with variable hydrothermal treatment times.

Regarding the supernatant collected after the treatment, the ICP analysis results are reported in Tab.5. While the concentration of YSZ components in the supernatant is minimal and

approximately negligible (worst case <450 ppm), the concentration of Nickel is very high and varies in a range between 7400 – 8800 ppm.

ICP quantitative elemental analysis [ppm]	Ni	Y	Zr
No HT HNO ₃	8.8 x 10 ³	19.4	408
HT2h HNO ₃	7.8 x 10 ³	9.2	151
HT4h HNO ₃	8.3 x 10 ³	7.3	179
HT12h HNO ₃	7.4 x 10 ³	5.2	53

Tab.5 – ICP analysis results on acid leaching supernatant.

The EDS semi-quantitative elemental analysis comparison between a pristine sample that was not treated either with hydrothermal or acid leaching treatment and a sample that underwent 4 h of hydrothermal processing and acid leaching is available in Fig.32. As it is possible to notice, in the latter, the molar fraction of Nickel becomes minimal.

EDS semi quantitative elemental analysis (molar%)

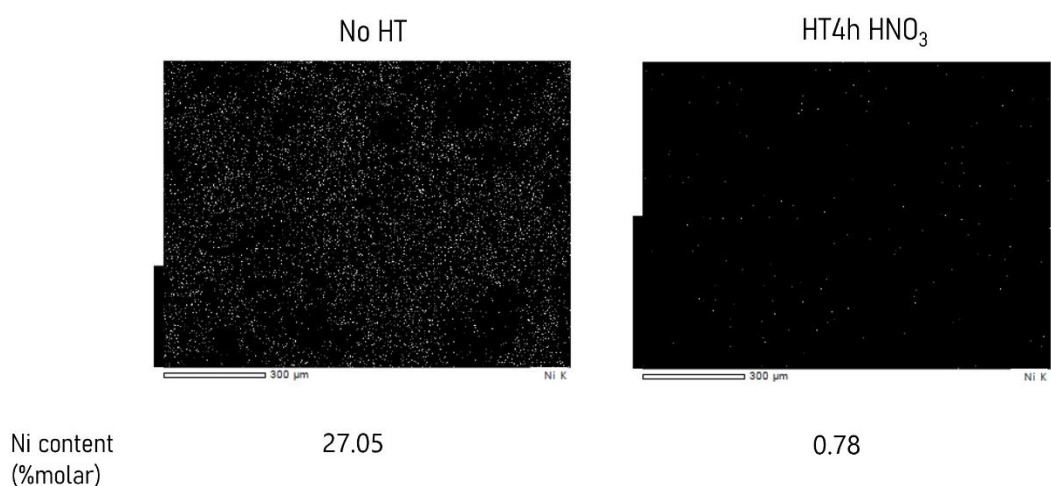


Fig.33 – EDS semi-quantitative elemental analysis: effect of HNO₃ on Nickel leaching.

Chelation

Chelation process was performed on samples of powders of 1 g in 50 ml of EDTA solution 0.8M with pH=11, at a temperature equal to 80°C and at stirring speed of about 600 rpm for 8 h. In Fig.33 the results from XRD analysis on powder samples with variable hydrothermal time treated with chelation are reported. The Nickel leaching occurs only partially since the corresponding peaks do not decrease in amplitude.

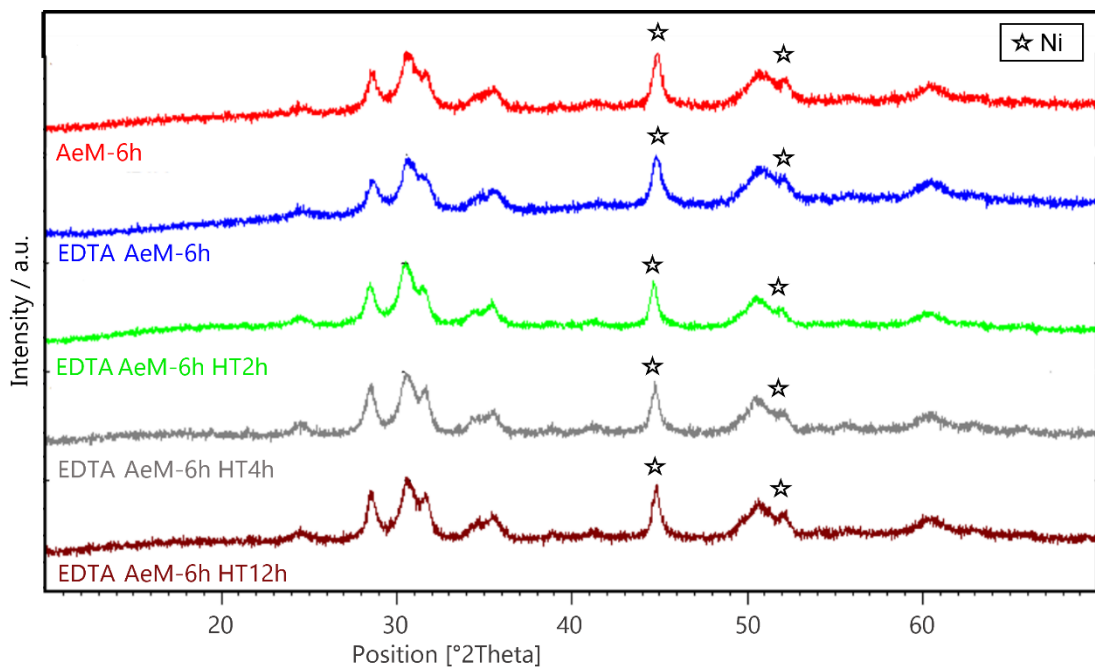


Fig.34 – XRD analysis: effect of chelation treatment on powder samples processed with variable hydrothermal treatment times.

ICP analysis results, reported in Tab.6, remark the low Nickel extraction effectiveness of this procedure, giving as an output a Nickel concentration in the supernatant that ranges approximately between 1700 – 2000 ppm. It is also worth noticing that this treatment causes a lower extraction of YSZ components if compared to HNO₃ leaching, given its milder effect.

ICP quantitative elemental analysis [ppm]	Ni	Y	Zr
No HT EDTA	1.74×10^3	0.2	0
HT2h EDTA	1.72×10^3	0.06	0
HT4h EDTA	2.04×10^3	0.04	0
HT12h EDTA	1.79×10^3	0.02	0

Tab.6 - ICP analysis results on chelation treatment supernatant.

In Fig.34 the comparison between a pristine sample that was not treated either with hydrothermal or chelation treatment and a sample that underwent 4 h of hydrothermal processing and chelation is proposed to additionally highlight the low performance in terms of efficiency of Nickel extraction.

EDS semi quantitative elemental analysis (molar%)

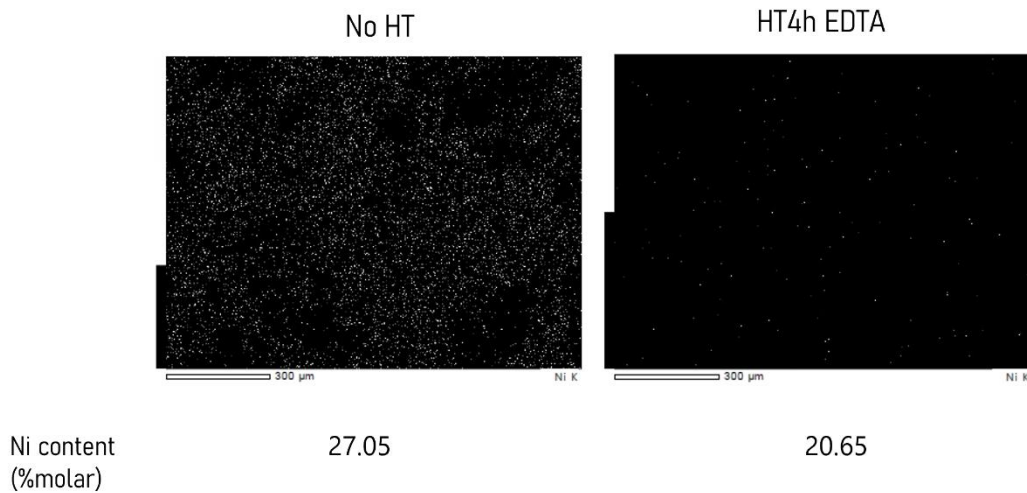


Fig.35 – EDS semi-quantitative elemental analysis: effect of EDTA chelation on Nickel leaching.

Although presenting as a milder alternative to acid leaching, chelation with EDTA does not seem to be enough efficient to justify the choice of this technique, at least in the particular

conditions of process adopted. A further investigation with increased time or temperature and in a closed reactor system could lead to a much more consistent result.

Mass balance

The whole process analyzed results in mass losses that are not negligible, with particular reference to some of the steps performed. The assessment was performed in terms of relative mass balance for each procedure, other losses such as losses due to dispersed powders during weighting were considered negligible in comparison.

The mass of the cells received from the supplier ranged from 22.5 to 23.0 g. Sealant removal procedure implied an average loss of 20% of the mass, although it is important to notice that only a portion of this value is an actual loss of cell material, since the sealant is not one of the target materials of the investigation. The assessment of the losses in the step in which cathode scratching and protective layer polishing were performed is not available since the scratching procedure adopted often resulted in a high cell fragmentation. In these conditions it was not possible to reconstruct each cell to perform weight analysis on each of them. Additionally, the procedure adopted to remove the GDC protective layer performed erosion of the latter, meaning it was not possible to assess if half-cell material (electrolyte and anode) was subjected to erosion along with the GDC layer. Therefore, only the global mass of all the fragments was measured to ensure the reference point in the analysis in the successive steps. Milling procedure average mass losses were in the order of 5%. In this step the main variation was due to the act of moving the powders while recovering, weighting and storing. Although the percentage value is limited, it is important to notice that in this step a fraction of the smallest-size powders was most likely dispersed. The most consistent losses occurred when it was necessary to retrieve the powders after hydrothermal and Nickel leaching treatments. The successive centrifugation procedure adopted to separate the powders from the supernatants led to mass losses in the order of magnitude of 30%.

In conclusion, as summarized in Tab.7, the most critical procedure in terms of mass losses is represented by the successive centrifugation, whereas, given the circumstances explained above, other procedures give a reasonable output value. Anyway, it is important to notice that even so, centrifugation procedure represented the most solid choice available when the separation and collection of both powders and supernatant was necessary.

Therefore, to improve the efficiency of the whole process it is important to reduce to the minimum the number of times in which it is needed to separate and collect both powders from supernatant. It is worth noticing that this was necessary for each step only in the experimental analysis optic, in order to assess the effect of the treatments. Another path that could be explored is the investigation of an alternative strategy to centrifugation. Additionally, concerning milling procedure, wet milling could also be implemented to avoid mass losses of small-size powders.

Procedure	Average weight losses [%]
Sealant removal	20%
Cathode scratching & polishing	-
Milling	5%
Centrifugation (hydrothermal & leaching treatments)	30%

Tab.7 – Average mass losses for each procedure adopted.

Conclusions

The experimental procedure implemented successfully applied hydrothermal methods to end-of-life SOFC anode material recovery, giving promising results.

The requirements in terms of specific surface area and particle size distribution provided by the industrial supplier were satisfied by processing the materials with hydrothermal treatment for 4 hours at 200°C in a closed reactor.

Additionally, the separation of Nickel from YSZ was successfully obtained by performing acid leaching with HNO₃ in the optic of new cells manufacturing. The study of the effect of acid concentration variation on the effectiveness of Nickel leaching could be carried out to determine the minimum concentration needed and further optimize the process.

Although chelation procedure did not seem to prove as effective, a further optimization of the treatment conditions could result in an overall better performance if compared with the data obtained.

The most critical procedure in terms of mass losses is represented by the successive centrifugation. In order to improve the efficiency of the whole process the direction to follow leads to a condition where the number of times where powders and supernatant are separated and collected is reduced to the minimum. In this context, the capability to perform combined treatments in a closed vessel designed for this purpose is of main interest. More in detail, the possibility to perform hydrothermal treatment together with acid leaching in the same reactor. The closed reactor should be designed to safely withstand high temperature, high pressure and acid environment to allow the treatment of a slurry of half-cells powders in a water solution with an optimized acid concentration, while possibly performing stirring to facilitate the reactions. The reaction vessel should be designed to minimize the thermal losses to reduce thermal energy consumption and keep the reaction temperature as stable as

possible. Wet milling procedure could be explored in order to avoid the dispersion of the smaller size fraction of the powders.

Although the need to conduct research to explore alternative procedures is evident in the optic of upscaling the process to industrial scale, at this stage manual cathode scratching and polishing represented the most pragmatic and available opportunity.

In terms of energy consumption, both mechanical and thermal energy are required. The main mechanical energy consumption is represented by successive centrifugations, along with milling and polishing procedure. As already highlighted, the reduction of the number of successive centrifugations performed in the process should result in reduced mass losses as well as suffice to contain an excessive utilization of mechanical energy. For what concerns milling, the optimized time obtained is 6 h, but it could be possible to reduce it while increasing hydrothermal treatment time and evaluate the energy balance in function of the time fraction of utilization of the two energy sources.

The thermal energy need is lower than the mechanical and it is linked to hydrothermal treatments and Nickel leaching procedures. Since both these procedures do not require a high temperature source, thermal insulation should suffice to limit thermal needs. An interesting application to optimize the industrial process could be the utilization of waste heat from the sintering process to feed the thermal need of the material recovery process to additionally stress its circularity and obtain an integrated system.

References

- [1] <https://best4hy-project.eu/>
- [2] Huang, Xinhong & Zhang, Zhihao & Jiang, Jin. (2006). *Fuel Cell Technology for Distributed Generation: An Overview*. IEEE International Symposium on Industrial Electronics. 2. 1613 - 1618. 10.1109/ISIE.2006.295713.
- [3] Norbert H. Menzler, Doris Sebold, Yoo Jung Sohn, Sebastian Zischke, Post-test characterization of a solid oxide fuel cell after more than 10 years of stack testing, *Journal of Power Sources*, Volume 478, 2020, 228770, ISSN 0378-7753, <https://doi.org/10.1016/j.jpowsour.2020.228770>.
- [4] Saad B.H. Farid, *Structure, microstructure, and properties of bioceramics*, Bioceramics: For Materials Science and Engineering, 2019
- [5] J. Chevalier, L. Gremillard, 1.106-Zirconia as a biomaterial, in: P. Ducheyne (Ed.), *Comprehensive Biomaterials*, Elsevier, Oxford, 2011, pp. 95–108. <https://doi.org/10.1016/B978-0-08-055294-1.00017-9>
- [6] H. Yanagida, K. Koumoto, M. Miyayama, *The Chemistry of Ceramics*, John Wiley & Sons, 1996. ISBN 0 471 95627 9.
- [7] Butz, Benjamin (2011). *Yttria-doped zirconia as solid electrolyte for fuel-cell applications: Fundamental aspects*. Südwestdt. Verl. für Hochschulschr. ISBN 978-3-8381-1775-1.
- [8] Hideko Hayashi, Tetsuya Saitou, Naotaka Maruyama, Hideaki Inaba, Katsuyuki Kawamura, Masashi Mori, *Thermal expansion coefficient of yttria stabilized zirconia for various yttria contents*, *Solid State Ionics*, Volume 176, Issues 5–6, 2005

- [9] Yang, Min et al. "Effects of chromium poisoning on the long-term oxygen exchange kinetics of the solid oxide fuel cell." *The Lancet* (2011)
- [10] Badwal, S., Deller, R., Foger, K., Ramprakash, Y., and Zhang, J. (1997). *Interaction between chromia forming alloy interconnects and air electrode of solid oxide fuel cells*. *Solid State Ionics* 99, 297–310. doi: 10.1016/S0167-2738(97)00247-6
- [11] Beez A, Schiemann K, Menzler NH and Bram M (2018). *Accelerated Testing of Chromium Poisoning of Sr-Containing Mixed Conducting Solid Oxide Cell Air Electrodes*. *Front. Energy Res.* 6:70. doi: 10.3389/fenrg.2018.00070
- [12] Kojima, T., Mori, Y., Kamiya, M. et al. Disintegration process of yttria-stabilized zirconia ceramics using hydrothermal conditions. *J Mater Sci* 42, 6056–6061 (2007).
<https://doi.org/10.1007/s10853-006-1167-4>
- [13] Antonio Valente, Diego Iribarren, Javier Dufour, End of life of fuel cells and hydrogen products: From technologies to strategies, *International Journal of Hydrogen Energy*, Volume 44, Issue 38, 2019, Pages 20965-20977, ISSN 0360-3199,
<https://doi.org/10.1016/j.ijhydene.2019.01.110>.
- [14] Hyuk Kim, Calvin da Rosa, Marta Boaro, John M. Vohs, and Raymond J. Gorte, *Fabrication of Highly Porous Yttria-Stabilized Zirconia by Acid Leaching Nickel from a Nickel-Yttria-Stabilized Zirconia Cermet*, *J. Am. Ceram. Soc.*, 85 [6] 1473–76 (2002)
- [15] Koteswara R. Vuyyuru, Kamal K. Pant, Venkatesan V. Krishnan, and Krishna D. P. Nigam, *Recovery of Nickel from Spent Industrial Catalysts Using Chelating Agents*, *Ind. Eng. Chem. Res.*, Vol. 49, No. 5, 2010
- [16] Peters, R. W. *Chelant extraction of heavy metals from contaminated soils*. *J. Hazard. Mater.* 1999, 66 (1-2), 151–210.

